NATIONAL RADIO ASTRONOMY OBSERVATORY
Green Bank, West Virginia

Electronics Division Internal Report No. 30

THE CHARACTERISTICS OF THE 300-FOOT TELESCOPE AT 10 CM WAVELENGTH

J. Baars and P. Mezger

MAY 1964

NUMBER OF COPIES: 100

THE CHARACTERISTICS OF THE 300-FOOT TELESCOPE AT 10 CM WAVELENGTH

Jaap W. M. Baars and Peter G. Mezger

1. Introduction

In a series of measurements which were started in order to obtain an experimental proof of some results of antenna tolerance theory, the NRAO 300-foot transit telescope was calibrated at $\lambda = 10$ cm. A total power receiver with a single channel noise figure of 1200 °K was mounted behind the focal point. Then the pointing error was determined and the horn feed focused in axial direction. The calibration marks (one with $\Delta T = 115$ °K and the other with $\Delta T = 43$ °K) were calibrated with loads at ambient temperature and at the temperature of liquid nitrogen, respectively.

The observations were started December 17th and terminated December 30th, 1963. Apart from the antenna calibration a series of tentative radioastronomical observations were made. The results of both the antenna measurements and the radioastronomical observations are presented in a working paper, of which only a very small number of copies exists. Since we think, however, that the performance of the 300-foot antenna will be of more general interest — especially since observations with improved receivers simultaneously at 11 and 21 cm wavelength are planned — that part of our working report which deals with the antenna calibration is published as an Electronics Division report. The figures in this report are numbered corresponding to their sequence in the working paper.

In section 2 the measurement of beam efficiency and aperture efficiency is described. In section 3 the concept of error pattern and some measurements related to this subject will be discussed. In section 4 we try to find a correlation between the measured antenna characteristics and the deformations of the mechanical structure of the 300-foot telescope at different zenith distances.

2. Measurement of Beam Efficiency and Aperture Efficiency

Having completed a pointing program with the 300-foot telescope in declination, we started with the measurement of drift curves through the center of the sources. The following drift curves were then spaced at certain distances $\Delta\delta$ in declination. Calibration marks were inserted at the beginning and the end of each drift curve.

Figure 1 shows a drift curve through Cas A with the intensity given in dB. Apart from the broadening effect due to the finite source diameter this curve is substantially a plot of the main beam pattern and the first sidelobes. Usually the HPBW of the antenna is obtained also from drift curves, using corrections for the finite source diameter. If both the source distribution and the main beam pattern can be approximated by gaussian functions, the observed antenna temperature distribution again is a gaussian function. In this case the HPBW of the antenna can be determined (if the source HPW's are known) even when the drift curve did not hit the center of the source. Unfortunately, the correction to be applied to an observed drift curve in order to obtain the HPBW of the antenna depends strongly on the source distribution. A survey of the literature [1] shows that the values obtained by various authors are not very consistent even in the case of the strongest radio sources. We decided to apply a different technique to determine the HPBW's of the 300-foot telescope at 10 cm. Two horn feeds — one for 10 cm and the other for 21 cm wavelength — were used both on the 85-foot and the 300-foot telescopes. In the case of the 85-foot telescope, the HPBW is so large that the effect of beam broadening does hardly depend on the source distribution. In the case of the 300-foot telescope, the effective antenna area at 21 cm wavelength is so large that point sources (3C 123, 3C 348 and 3C 353) could be used to determine the HPBW's. Then the HPBW of the 300-foot antenna at $\lambda = 10$ cm has been calculated using the relation

$$\Theta_{A300}(\lambda_1) : \Theta_{A300}(\lambda_2) = \Theta_{A85}(\lambda_1) : \Theta_{A85}(\lambda_2)$$

$$\lambda_1 = 21 \text{ cm}; \quad \lambda_2 = 10 \text{ cm}$$

and obtained

(1a) $$\Theta_{A300}(\lambda_2) = 4.4' \qquad \text{(focused antenna)}$$

In another independent method drift curves over the disk of the moon were used to obtain the antenna HPBW [2]. Such drift curves were measured between declination angles $-14° \leq \delta \leq +22°$. It turned out that the 300-foot antenna was strongly defocused at low declination angles and became gradually better focused with increasing elevation angle. Figure 2 shows the average value of two drift curves measured at $\delta = 20.5°$ and 22°, respectively (full curve). The evaluation of this curve led to

(1b) $$\Theta_A = 4.75' \pm 0.25' \qquad \delta = 21°$$

From drift curves of Virgo a HPBW of

(1c) $$\Theta_A = 4.9' \qquad \delta = 12.6°$$

was calculated assuming a HPW of Virgo in RA $\approx 1'$. As will be shown in section 4 the feed was defocused at $\delta = 12.6°$ by about 5 cm which leads to a theoretical beam broadening of +0.3'. This means that the three values, 1a, b and c, obtained by independent methods are compatible. All these measurements were only made in right ascension for one given feed polarization, namely, the electric vector parallel to the NS-direction. From the fact that the feed produced a circular main beam at the same wavelength in the 85-foot telescope, it was concluded that the main beam of the 300-foot telescope was circular also.

Using the measured drift curves, the contour maps (figs. 5, 8, 11, and 14 of Cas A, Cyg A, Tau A and Virgo A were drawn and then numerically integrated over the main beam area. Table 1 lists the results of these computations.

Table 1

Source	$\frac{S(source)}{S(Cas\ A)}$ (Heeschen [3])	$S_{3\ GHz}$ in $W/m^2\ Hz$	T_A max in °K	$\int T_A\, d\Omega$ in °K (min of arc)^2	$\frac{S(source)}{S(Cas\ A)}$	η_B
Cas A	1.00	$130.0 \cdot 10^{-25}$	250	6966	1.00	0.126
Cyg A	0.481	$62.5 \cdot 10^{-25}$	142	3421	0.491	0.128
Tau A	0.510	$66.3 \cdot 10^{-25}$	120	3657	0.524	0.129
Virgo A	0.077	$10.0 \cdot 10^{-25}$	17	422.4	0.061	0.099

The second column gives the relative flux of the sources as measured by Heeschen [3]. The absolute flux values in column 3 were obtained using the relative fluxes and the absolute flux $S_{1.44\ GHz}(Cas\ A) = 233.5 \times 10^{-25} \pm 5\%\ W/m^2Hz$ (preliminary values of Findlay and Hvatum, private communication) and assuming a spectral index of -0.8.

The following columns (4-7) list our results. In column 4 the maximum observed antenna temperatures, in column 5 the antenna temperatures integrated over the main beam area, and in column 6 the relative flux values calculated from the values of column 5 are given. These last values agree well with Heeschen's results (column 2). Only our value for Virgo is too small, which again can be explained by the defocusing of the 300-foot antenna at low declination angles (see section 4).

Using the relation

$$S_\nu = \frac{2k}{\lambda^2} \int_{\text{main beam}} T_s \, d\Omega = \frac{2k}{\lambda^2 \eta_B} \int\int_{\text{main beam}} T_A(\xi, \eta) d\xi d\eta \tag{2}$$

and the values of table 1, we finally obtained the main beam efficiency listed in column 7 The mean value of the first three sources is

$$\eta_B = \eta_R(1 - \beta_m) = 0.128 \pm 0.01 \tag{3}$$

and the corresponding aperture efficiency is

$$\eta_A = 0.105 \pm 0.01 \tag{4}$$

The absolute antenna temperature with the antenna pointed at zenith was found to be $T_A(\text{zenith}) = 47\ ^\circ K$ at 3 GHz, as compared to a value of 31 °K measured at $\lambda = 1.4$ GHz. The increase of the zenith antenna temperature at 3 GHz is partially due to the increased transmission of the 5/8" square mesh reflector surface at this frequency. Different measurements lead to transmission coefficients of 2.5 and 4.5%, respectively, of the mesh at $\lambda = 10$ cm.

The beam efficiency of the 300-foot antenna decreases from $\eta_B = 0.53$ at 1.4 GHz to $\eta_B = 0.13$ at 3 GHz, whereas the antenna temperature measured at zenith remained constant apart from the contribution due to the increased reflector transmission at 3 GHz.

This is in agreement with the predictions of Ruze [4] and Scheffler [5] concerning the error pattern, caused by random deviations of the reflector (see section 4).

The radiation temperature of the moon at $\lambda = 10$ cm is nearly constant and independent on the phase of the moon, $T_M = 230$ °K. The antenna temperature of the moon, measured with the 300-foot telescope at $\lambda = 10$ cm at declination angles of about 20°, has been found to be 39.5 °K. We will denote the main beam efficiency, obtained from these values, by

(5) $$\eta_B' = 39.5/230 = 0.173$$

For Tau A, which has a similar declination angle, we have obtained a main beam efficiency $\eta_B = 0.129$ (see table 1); η_B' is larger by 0.044 or 34%. This difference is due to the fact that in the case of the moon not only the main beam but also the stray region in the neighborhood of the main beam receives a considerable amount of the moon's radiation. This fact can be used to calculate the average attenuation of the first sidelobes. About four sidelobes are contained in the solid angle with the diameter of the moon's disk. Using an earlier calculation [6] the antenna solid angle of the main beam and the first sidelobes can be written in the form

$$\Omega' = \Omega_m \left\{ 1 + 1.4 \sum_{i=2}^{4} a_i [2.1 + (i - 2)] \right\}$$

with Ω_m the main beam solid angle and $a_i = f_i$ the amplitude of the i-th sidelobe of the power pattern. With the assumption $a_1 = a_2 = \ldots = a$, one obtains $\Omega' = \Omega_m(1 + 13a)$. Then the relation

$$\Omega_m/(\Omega' - \Omega_m) = \eta_B/(\eta_B' - \eta_B) = 1/13a = 0.129/0.044 = 2.93$$

leads to

(6) $$a = 1/38 = -15.8 \text{ dB}$$

for the average attenuation of the first four sidelobes, this result being compatible with

our direct measurements of the power pattern (fig. 1). It will be shown in section 3 how this difference in the main beam efficiencies η_B and η_B', respectively, can be used to obtain more information on the error pattern.

3. The Error Pattern

Ruze [4] obtained the result that gain and aperture efficiency of an antenna decreases with $\exp\left\{-\overline{\delta^2}\right\}$. $\sqrt{\overline{\delta^2}}$ is the RMS phase error introduced by the surface deviations of the reflector from the best fitting paraboloid. RMS surface deviation $\overline{d^2}$ and RMS phase error are related by

$$\overline{\delta^2} = 16\,\pi^2\,\frac{\overline{d^2}}{\lambda^2} \tag{7}$$

The RMS phase error not only decreases gain and aperture efficiency but also increases the relative level of the first sidelobes. The resulting pattern then can be represented by the sum of the diffraction pattern $f_o(\Theta)$ and an error pattern. Neglecting the obliquity factor $S(\Theta)$, putting $\sin\Theta \approx \Theta$ and replacing Ruze's notation of the correlation interval C of the random surface deviations by ℓ, one can write Ruze's result in the form

$$f(\Theta) = f_o(\Theta) + \frac{4\pi^2\ell^2\delta^2}{\lambda^2\,G_o}\sum_n \frac{1}{n\,!\,n}\,[\overline{\delta^2}]^{n-1}\exp\left\{-\frac{\pi^2\ell^2\Theta^2}{n\lambda^2}\right\} \tag{8}$$

G_o is the gain of the undisturbed ("no error") reflector. This sum of exponential functions is not very convenient for calculation. Now Scheffler, in an independent investigation of the required surface accuracy of optical telescopes [5], has introduced the approximation

$$\exp\ \overline{\delta^2}\,[1 - e^{-x^2/\ell^2}] = \begin{cases} (1 - e^{-\overline{\delta^2}})\,e^{-x^2/\ell^2} + e^{-\overline{\delta^2}} & \text{for } \overline{\delta^2} \leq 1 \\ (1 - e^{-\delta^2})\,e^{-\delta^2\,x^2/\ell^2} + e^{-\overline{\delta^2}} & \text{for } \overline{\delta^2} \geq 1 \end{cases} \tag{9}$$

and obtained the approximation

$$(10) \qquad f(\Theta) = f_o(\Theta) + (e^{\overline{\delta^2}} - 1)\,\frac{4\pi^2\ell^2}{\lambda^2 G_o} \cdot \begin{cases} \exp\left\{-\pi^2\ell^2\Theta^2/\lambda^2\right\} \\ \\ \dfrac{1}{\overline{\delta^2}}\exp\left\{-\pi^2\ell^2\Theta^2/\lambda^2\overline{\delta^2}\right\} \end{cases}$$

for the resulting pattern.*

Neglecting the sidelobes of the diffraction pattern the total antenna pattern is composed of two gaussian beams. The diffraction pattern main beam has a HPBW of (valid for an edge tapering of $\approx 16 \div 18$ dB)

$$(11) \qquad \frac{\Theta_A}{\text{min of arc}} \doteq 4.176 \cdot 10^3\,\lambda/D$$

(D diameter of the circular aperture). The error pattern has a HPBW of

$$\Theta_e = 2\sqrt{\ln 2} \cdot \begin{cases} \lambda/\pi\ell & \overline{\delta^2} \leq 1 \\ & \text{in radian} \\ \lambda\sqrt{\overline{\delta^2}}/\pi\ell & \overline{\delta^2} \geq 1 \end{cases}$$

or

$$\frac{\Theta_e}{\text{min of arc}} = \begin{cases} 1.822 \cdot 10^3\,\lambda/\ell & d \leq \lambda/12.566 \\ \\ 2.290 \cdot 10\ d/\ell & d \geq \lambda/12.566 \end{cases}$$

The ratio of the HPBW of the error pattern to the HPBW of the diffraction pattern is

$$(13) \qquad \frac{\Theta_e}{\Theta_A} = \begin{cases} 0.436\ D/\ell \\ \\ 5.484\ D\sqrt{d^2}/\lambda\ell \end{cases}$$

---

* Scheffler has made his investigation for the case of optical telescopes. We had, consequently, to adjust his results so that they correspond to the definitions and notations used in radio antenna theory.

For Θ/radian $\ll \lambda/\pi\ell$ or Θ/min of arc $\ll 1.09 \cdot 10^3 \frac{\lambda}{\ell}$ the decrease in the sidelobe level is

$$(14) \qquad \left[e^{16\pi^2 \frac{\overline{d^2}}{\lambda^2}} - 1 \right] x \begin{cases} \frac{4\ell^2}{\eta_A D^2} & d \leq \lambda/12.566 \\ \frac{1}{\eta_A 4\pi^2} \left(\frac{\ell\lambda}{D\sqrt{\overline{d^2}}} \right) & d \geq \lambda/12.566 \end{cases}$$

Integrating the total error pattern both expressions, equation (8) and the approximation (10), yield the same result

$$(15) \qquad \int_{4\pi} f d\Omega = \Omega = \Omega_o + (e^{\overline{\delta^2}} - 1)\Omega_o = \Omega_o e^{\overline{\delta^2}}$$

Ω_o is the antenna solid angle of the undisturbed pattern. This result means that the total antenna solid angle is increased by the same amount that the gain and efficiency of the antenna are decreased. The main beam stray factor becomes

$$(16a) \qquad \beta_m = 1 - \Omega_m \Omega = 1 - \frac{\Omega_m}{\Omega_o} \cdot e^{-\delta^2}$$

The beam efficiency becomes

$$(16b) \qquad \eta_B = \eta_R(1 - \beta_m) = \eta_R \frac{\Omega_m}{\Omega_o} e^{-\overline{\delta^2}} = \eta_{B_o} e^{-\overline{\delta^2}}$$

provided that the radiation efficiency η_R is independent of frequency. These results enable us to calculate the difference in beam efficiency, measured either with a point source (yielding η_B) or measured with an extended source like the moon (yielding the efficiency η_B'). As was shown in section 2, the beam efficiency η_B' is greater than η_B since part of the error pattern receives too much radiation from the extended source.*

* The level of the sidelobes of the pure diffraction pattern are in most cases so low that their contribution to the beam efficiency in this case can be completely neglected.

If the beam efficiency is measured with a point source, the contribution of the error pattern can be neglected and one finds $\eta_B \sim \Omega_m$. If the source is extended the integration of the antenna pattern over the solid angle subtended by the source includes a contribution of the error pattern

$$\int_{\text{solid source angle}} f \, d\Omega = \Omega_m + \int_{\text{solid source angle}} f_e \, d\Omega$$

Assuming a circular source with diameter 2R, the integration of equation (26) can be performed. With η_{B_o} the beam efficiency of the undisturbed reflector, η_B the beam efficiency of the disturbed reflector, measured with a point source, and η_B' the beam efficiency measured at the same wavelength but with an extended circular source with apparent diameter 2R, we find eventually

$$(17) \qquad \frac{\eta_B' - \eta_B}{\eta_{B_o} - \eta_B} = \begin{cases} 1 - \exp\left\{-\dfrac{\pi^2 \ell^2 R^2}{\lambda^2}\right\} & d \leq \lambda/12.566 \\ 1 - \exp\left\{-\dfrac{\ell^2 R^2}{16\, \overline{d^2}}\right\} & d \geq \lambda/12.566 \end{cases}$$

The source radius has to be inserted in radian. In most practical cases the left side of equation (17) is a value << 1 so that we can write

$$(18) \qquad \ell = \left[\frac{\eta_B' - \eta_B}{\eta_{B_o} - \eta_B}\right]^{1/2} \cdot \begin{cases} 1.094 \cdot 10^3 \, \lambda/R & d \leq \lambda/12.566 \\ 1.375 \cdot 10^4 \sqrt{d^2}/R & d \geq \lambda/12.566 \end{cases}$$

with R, now, to be inserted in min of arc.

In order to compare these theoretical predictions, we compile the RMS reflector deviations, measured by a photogrammetric method and weighted for the feed pattern, in the following table:

Table 2

Zenith angle	0°	30°	51° 24'
Weighted RMS deviation [8] $\sqrt{\overline{d^2}}$	12.44 mm	12.63 mm	10.87 mm

By measurements with the moon and with Tau A, respectively, at about the same declination, we obtained the values $\eta_B = 0.129$ and $\eta_B' = 0.173$. By extrapolating earlier measurements [8] we find for the beam efficiency of the undisturbed 300-foot reflector $\eta_{B_o} = 0.88$. With these values the correlation length of the random surface deviations can be calculated. Since $\lambda/12.566 = 8$ mm the relation holds

$$\mathcal{L} = 2.42\ 10^{-1} \times 1.375\ 10^{4} \times \frac{12}{16}\ 10^{-3} = 2.5 \text{ meters}$$

(R = 16' is the half diameter of the moon.) Inserting this value in equation (12) we find a HPBW of the error pattern of 110 min of arc. The level of the maximum of the error pattern relative to the maximum of the diffraction pattern ($f_o(0) = 1$), calculated from equation (14) comes out to be

$$\text{(19)} \qquad \begin{matrix}\text{relative level of} \\ \text{the errors pattern}\end{matrix} = 2.42 \cdot 10^{-2} = -16.2 \text{ dB}$$

This is in agreement with the measurements of the power pattern (fig. 1) as well as with our previous calculation of the average attenuation of the first sidelobes (eq. 6). The values enable us to calculate the drift curve of the moon through the error pattern. The HPW of this drift curve is about identical with the HPBW of the error pattern, $\Theta_e = 110'$. The maximum antenna temperature is obtained by equating the convolution integral $T_A = T_M \frac{1}{\Omega} \int (f_o + f_e) d\Omega$ over the disk of the moon. This leads to

$$(20) \qquad T_A = T_M \left[\eta_B + \left(1 - \exp\left\{-\frac{16\pi^2\overline{d^2}}{\lambda}\right\}\right)\left(1 - \begin{cases} \exp\left\{-\frac{\pi^2\ {}^2R^2}{\lambda^2}\right\} & d \leq \frac{\lambda}{12.566} \\ \exp\left\{-\frac{{}^2R^2}{16\,d^2}\right\} & d \geq \frac{\lambda}{12.566} \end{cases}\right)\right]$$

The measured value of the beam efficiency is $\eta_B = 0.13$. Inserting the values obtained in the previous calculations we finally obtain $T_A = T_M\,(0.13 + 0.05)$. With $T_M = 230$ °K we find the resulting antenna temperature of the moon is 41.5 °K where the equivalent radiation power of 30 °K is received by the main beam of the diffraction pattern and 11.5 °K by the error pattern. This agrees with the experimental results and may serve as a check for our calculations.

Figure 23 shows the diffraction pattern and the error pattern of the 300-foot telescope at $\lambda = 10$ cm. The sidelobes of the diffraction pattern have been omitted for the sake of simplicity. As may be seen, however, by inspecting the contour maps of Tau A (fig. 11) or of Virgo A (fig. 14) the assumption of a gaussian error pattern must be modified for lower declination angles. The subsidiary maxima appearing in these contour maps are displaced images of the main lobe, caused by a periodic distortion of the reflector. It is interesting to notice that the same subsidiary maxima occur already in the 300-foot antenna pattern at 1420 and 750 MHz, respectively (fig. 24).

It is known that a periodic phase error with the "spatial wavelength" $p = D/m$ (D = diameter of the aperture) across the aperture will cause two equal sidelobes on either side of the main beam at an angular distance $m\lambda/D$ radian (λ = wavelength). Then m is the number of cycles of phase error along the aperture. The amplitude of the subsidiary maxima relative to the main beam is equal to one-half the peak phase error, expressed in radians. Applying these results to the measured antenna pattern figure 24 leads to a wavelength of the periodic phase error of about 44 meters and an amplitude of about 0.6 radian corresponding to a surface deviation of about 5 mm.

4. The Effect of an Axial Defocusing of the Feed

This effect has been studied theoretically by Cheng [9]. He calculates the gain reduction as a function of the maximum phase deviation m from an average value, defined by the equation

$$|\Delta\Phi(x)| = |\Phi(x) - \Phi(x)| \leq m \tag{21}$$

$\Phi(x)$ is the phase function of the aperture field distribution; the variable x runs from -1 to +1. The gain variation is then

$$G/G_o = (1 - m^2/2)^2 \approx 1 - m^2 \tag{22}$$

By comparison with another and experimentally checked result for the gain reduction due to an axial defocusing [8] we find that*

$$m = \frac{1}{\sqrt{3}} \frac{\Delta f_{ax}}{\lambda} (1 - \cos \Theta_o) \tag{23}$$

with Θ_o the aperture angle.

This gain reduction is a result of beam broadening as well as of an increase in the sidelobe level. Whereas the increase in the sidelobe level can be best obtained by computing a set of far field patterns as a function of the feed position, Cheng [9] has derived a formula for the beam broadening, again as a function of the maximum phase deviation m.

$$\Delta u = \frac{m^2}{2} \left[\frac{g(u)}{-\frac{d}{du} g(u)} \right]_{u_o} \tag{24}$$

---

* We can also calculate the difference in path length for the central and edge ray in the case of a defocused feed, which yields $k\Delta l_{max} = 2\,\Delta f_{ax}(1 - \cos \Theta_o)/\lambda$. The phase error at a distance x of the center is then $\Delta l = x\Delta l_{max}$ and the mean value $(\overline{x^2} - \overline{x}^2)^{1/2} = 1/3\sqrt{2}$ which leads to a slightly smaller value than equation (23).

g(u) is the voltage pattern, $u = \frac{\pi D}{\lambda} \sin \Theta$, u_o is the value of the variable at half power width. Introducing the gaussian approximation for main beam pattern, we find $\Delta\Theta_A = m^2\, 0.72\, \Theta_A$. If $\Theta_A' = \Theta_A + \Delta\Theta_A$ is the HPBW of the broadened beam, Θ_A the HPBW of the focused beam, the relation holds

$$(25) \qquad \Theta_A' = \Theta_A [1 + 0.72\, m^2] = \Theta_A \left[1 + 2.36 \left(\frac{\Delta f_{ax}}{\lambda}\right)^2 (1 - \cos \Theta_o)^2\right]$$

In the case of the 300-foot telescope f/D = 0.428 and from $\mathrm{ctg}(\Theta_o/2) = 4f/D$ follows $\Theta_o = 60°$, $\cos \Theta_o = 0.5$ and equation (25) becomes $\Theta_A' = \Theta_A \left[1 + 0.59 \left(\frac{\Delta f_{ax}}{\lambda}\right)^2\right]$. We finally apply this formula to our observation of Virgo A with the 300-foot telescope. The declination of Virgo is 10°, corresponding to a zenith distance of z = 26°. At this distance the gain has been reduced to 0.845. Inserting this value in equation (22) we find $m^2 = 0.155$ and, from equation (25), $\Theta_A'/\Theta_A = 1.12$. Since $\Theta_A = 4.4'$ the HPBW at the zenith distance of Virgo is 4.9' in good agreement with the experimental result. The corresponding axial defocusing is $\Delta f_{ax} = 0.45\lambda = 4.5$ cm.

5. Correlation Between High Frequency Characteristics and Deformations of the Mechanical Structure of the 300-Foot Telescope

We start with a short description of the mechanical structure of the telescope. The feed is supported by two legs, lying in the NS-plane. The base of the triangle formed by these legs is 160 feet = 49 meters. The legs themselves are substantially a steel lattice with a width of 2 feet 10 inches = 0.85 meter. The basic structure of the reflector are segments with a base length of 38 feet = 11.6 meters. The back-structure is made up of radial conduits and nearly concentric bandings, which are connected to the bearing structure by means of studs. There are selected studs, whose position has been carefully computed and adjusted in order to form points of the designed parabolic shape of the reflector. The main radial conduits, which are tied to these studs, form consequently chords of the true paraboloid. The concentric bandings are then fastened to the conduits, their radial spacing being about 2.5 feet = 76.5 cm. The average radial spacing of the adjusted studs is 20 feet = 6.1 meters; the average distance between these studs on the reflector surface is about 2.83 meters.

The proper reflecting surface is formed of aluminum mesh 1.6 x 0.2 cm, which has been cut in panels, after having been fastened to the concentric bandings. The radial dimension of the panels is 5 feet = 1.53 meters; this means that each panel is not only supported at the edges but also in its radial center by one of the bandings. A typical segment consists of 78 panels. The first 6 panels are arranged in a single row; the following 16 panels are arranged in two rows of 8 panels; the following 56 panels are arranged in four rows of 14 panels. The weighted mean lateral dimension of the panels is 7.5 feet = 2.3 meters; the average dimension of the panels both in lateral and radial direction is 1.9 meters.

The reflector surface has been measured at three different zenith distances using a photogrammetric method. (This work has been done by D. Brown Associates, Inc., Eau Gallie, Florida.) We have calculated the weighted RMS deviations [8] which are given in table 2. Figures 26a, b, and c show a contour map representation of the reflector deviations. (In the original contour maps, drawn by D. Brown Associates, there is some confusion concerning the zero lines. We have tried to correct these errors so that our contour maps differ slightly from the original ones.) The regions of negative deviations, i.e., in a direction opposite to the focal point, are shadowed. One notices that at z = 0° the deviations seem to be randomly distributed, but become more systematic with increasing zenith distance, showing a clear astigmatism at low declination angles (fig. 26 b and c).

The deflection of the feed support in axial and radial direction with respect to the rigid back structure of the telescope has been measured by Sidney Smith. The results of these measurements are shown in figures 25a and b. With increasing zenith distance the feed support is deflected both towards the vertex of the reflector and towards the horizon.

In the following we try to correlate some of the high frequency characteristics of the 300-foot telescope with its mechanical structure and mechanical characteristics, respectively.

I. Irregularities in the First Sidelobes

Figure 1 shows the antenna pattern in EW-direction. The expected position of the first three sidelobes is indicated. The most striking feature is the obvious suppression of the second sidelobe. Considering the effect of aperture blocking by the feed support legs in NS-direction means that the voltage pattern of the corresponding aperture has to be subtracted from the far field pattern of the circular aperture. It is then clear that the odd sidelobes (equal phase) will be reinforced; the even sidelobes will be decreased (opposite phase) as is shown in figure 1.

II. The Errors Pattern Caused by the Random Reflector Deviations

We have evaluated our measurements for the case of a random distribution of the surface deviations, and obtained as a result a gaussian error pattern with a HPW of 110 min of arc, a relative raise of the level of the first sidelobes by about 16 dB and a correlation length of the deviations of 2.5 meters. With these values the drift curve of the moon has been calculated (eq. 35). Comparing the expected drift curve with the observed drift curve (fig. 2), it seems that the HPW of the error pattern is even narrower and that the error pattern may deviate considerably from the gaussian form (fig. 11) at least at large zenith distances.

The calculated correlation length of 2.5 m corresponds approximately both to the average length of the reflector panels of 1.9 meters and to the average distance of 2.3 meters of the studs, which has been adjusted to the designed parabolic shape, respectively.

III. The Periodic Surface Deviations

Figure 24 shows the antenna pattern, measured at three different wavelengths and a zenith distance of about 20° to the south. The general feature-distance of the subsidiary maxima proportional to wavelength, their intensity inversely proportional to wavelength— are typical for a periodic surface deviation. This periodic deviation apparently is limited to only one-half of the reflector surface. The symmetry of the

subsidiary maxima with respect to the NS-direction as well as a periodicity of 44 meters (nearly one radius of the aperture) hints that this may be caused by an elliptic deformation with its symmetry axis in NS-direction.

An inspection of the contour maps (figs. 26b and c) reveals clearly such a large scale deviation of the reflector at low declination angles. The radial size of the shadowed areas (i.e., with negative deviations) is very close to 44 meters; their position is approximately symmetrical with respect to the NS-line. The negative deflections on the west side are stronger than the negative deflections on the east side. It is obvious that a negative deflection of the reflector corresponds to a tilt of the main beam in the same direction. The appearance of the two subsidiary maxima in the antenna pattern (fig. 24) can therefore be related at least qualitatively to the deformation of the reflector.*

IV. Defocusing

A defocusing due to a mechanical deformation of the feed support legs has been anticipated. The change of the feed position has been measured using a theodolite, which has been mounted to the rigid part of the back-structure. Both the lateral and axial movement of the focal point as a function of zenith distance z is plotted in figure 25. With increasing zenith distance the focal points move toward the reflector (fig. 25a), and towards the horizon (fig. 25b). The axial defocusing causes a fattening of the main beam and a reduction of the effective antenna area, whose effects have been clearly found when measuring Virgo A at a zenith distance of about 30°. But the corresponding axial defocusing of 4.5 cm is much larger than the deviation which has been measured at that zenith distance.

A radial defocusing towards the horizon tilts the beam in the opposite direction, the angle between the electrical and mechanical axes being about 0.85 times the angle between the mechanical axis and the phase center of the defocused feed. This effect tends in the same direction as the atmospheric refraction does. Taking a pointing program made by Wade for $\lambda = 20$ cm and subtracting the effect of refraction we have

---

* Comparing figure 24 with the contour map, figure 11, of Tau A one should bear in mind that East and West must be reversed when the transition from the source contour map to the contour representation of antenna pattern is made.

calculated the corresponding radial defocusing (fig. 25b) which turns out to be considerably stronger than the lateral deflection of the phase center relative to the rigid back-structure of the reflector. Apparently not only the feed support legs but also the reflector is deformed by the gravitational force. Both effects tend to deflect the electrical axes of the 300-foot reflector in the same direction. This also may explain the much stronger gain reduction and fattening of the main beam than would be anticipated only from the axial defocusing due to the sag in the feed support legs.

V. The Fine Structure of the Surface Deviations as Obtained from Photogrammetrical Calibration

It is known from the photogrammetric calibration of the 300-foot reflector that not only the RMS surface deviation but also the focal length of the best fitting paraboloid changes with zenith distance. There are two reasons why the attempt may fail to correlate the high frequency characteristics measured as a function of zenith distance with the photogrammetric measurements:

1. The photogrammetric method yields only the focal length of the best fitting paraboloid, but does not give the position of the corresponding focal point with respect to a fixed point on the telescope. Also, one has to discriminate between the focal length of the best fitting paraboloid and the effective electrical focal length, which would be obtained by weighting the measured deviations of the target points with the feed power pattern.

2. For the calibration of the 300-foot reflector the position of the 293 target points on the reflector have been measured. If these points were equally spaced on the reflector surface, the average distance between two target point would be about 5 meters, that is, two times the correlation length of the surface deviations as found by high frequency measurements. It is quite clear, therefore, that the RMS

2. (continued)

deviations of the surface as obtained from the photogrammetric calibration can be correlated with the high frequency characteristics but that an attempt to correlate the photogrammetrically determined structure of the reflector with irregularities in the far field pattern will fail.

References

[1] Ng, W. W. and Keen, N., "A Survey of Radio Sources and the Possibility of Observing Them With the NRAO Interferometer", NRAO Internal Report (November 1963).

[2] Stumpff, P., in preparation.
and Meredith, B. L.

[3] Heeschen, D. S., "Observations of Discrete Sources at 40 and 10 cm Wavelength", NRAO Publ. No. 8 (1961).

[4] Ruze, J., "Physical Limitations on Antennas", Techn. Report 248, Research Laboratory of Electronics, MIT (October 30, 1952).

[5] Scheffler, H., "Ueber die Genauigkeitsforderungen bei der Herstellung optischer Flaechen fuer astronomische Teleskope", Z.f. Astrophys 55, 1-20 (1962).

[6] Mezger, P. G., "Principle Considerations of Radioastronomical Observations at Very High Frequencies", Internal Report of NRAO (March 1964).

[7] Mezger, P. G. and Stumpff, P., "The Measurement of the Diameter of Radio Sources With Pencil Beam Antennas", NRAO Electronics Division Internal Report No. 16 (August 1963).

[8] Mezger, P. G., "Application of Antenna Tolerance Theory to the NRAO 85-Foot and 300-Foot Telescopes", NRAO Electronics Division Internal Report No. 17 (August 1963).

[9] Cheng, D. K., "Effect of Arbitrary Phase Errors on the Gain and Beamwidth Characteristics of Radiation Pattern", IRE Transactions AP-3, 145-147 (1955).

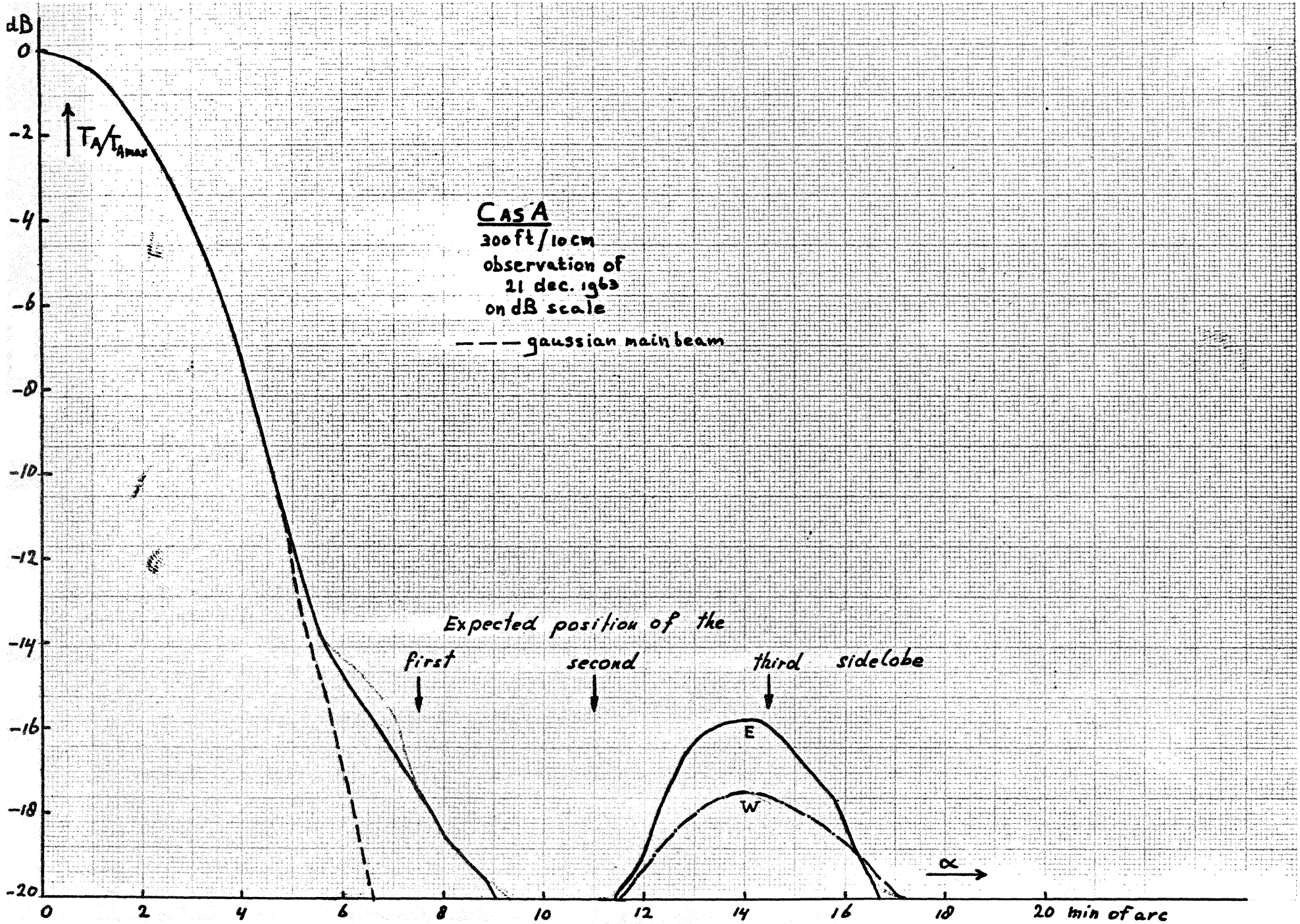

Fig. 1: Drift curve of Cas A through the magnetic plane of the antenna. Normalized antenna temperature in dB versus angular distance from the electrical axis.

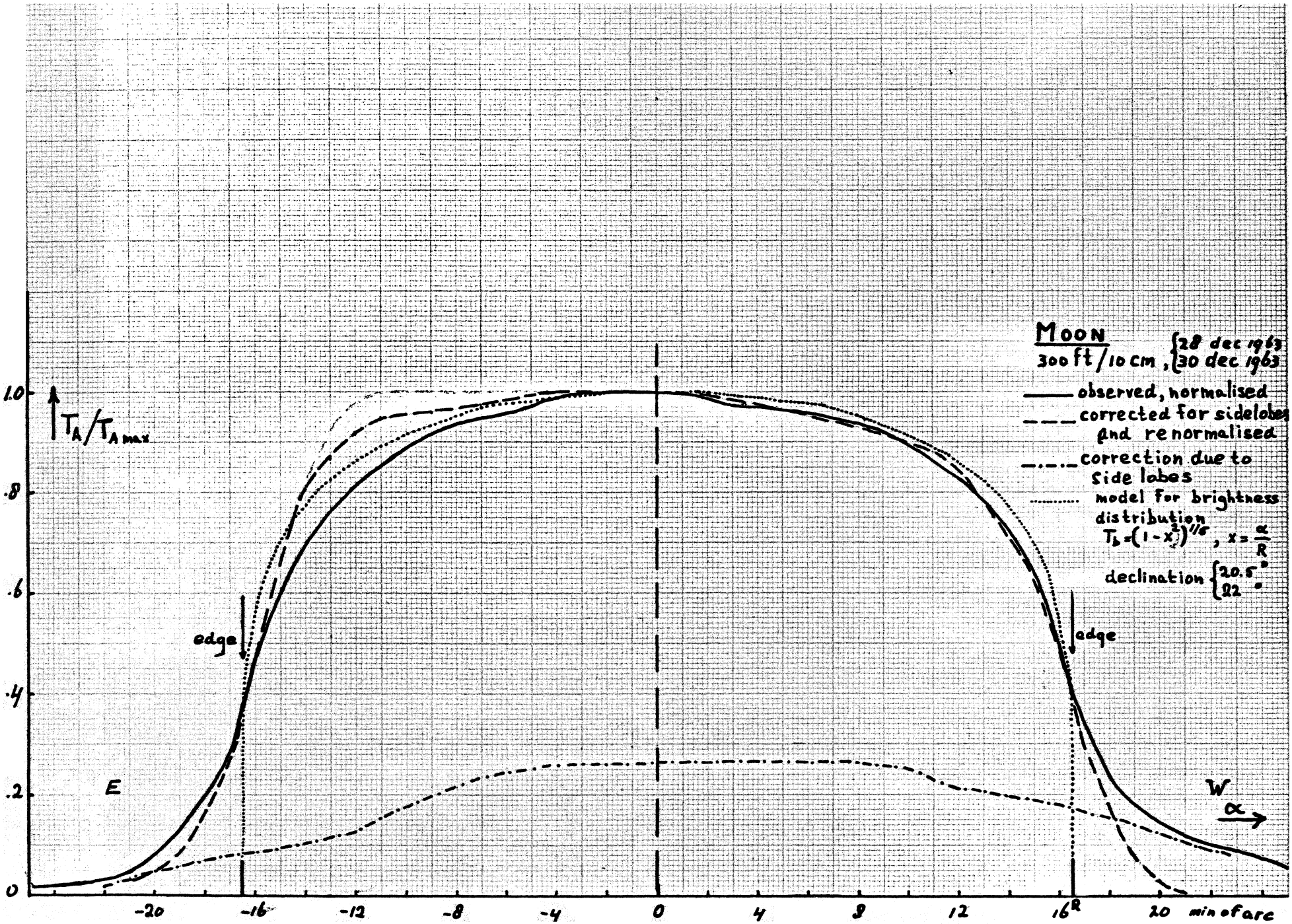

Fig. 2: Drift curve of the moon.

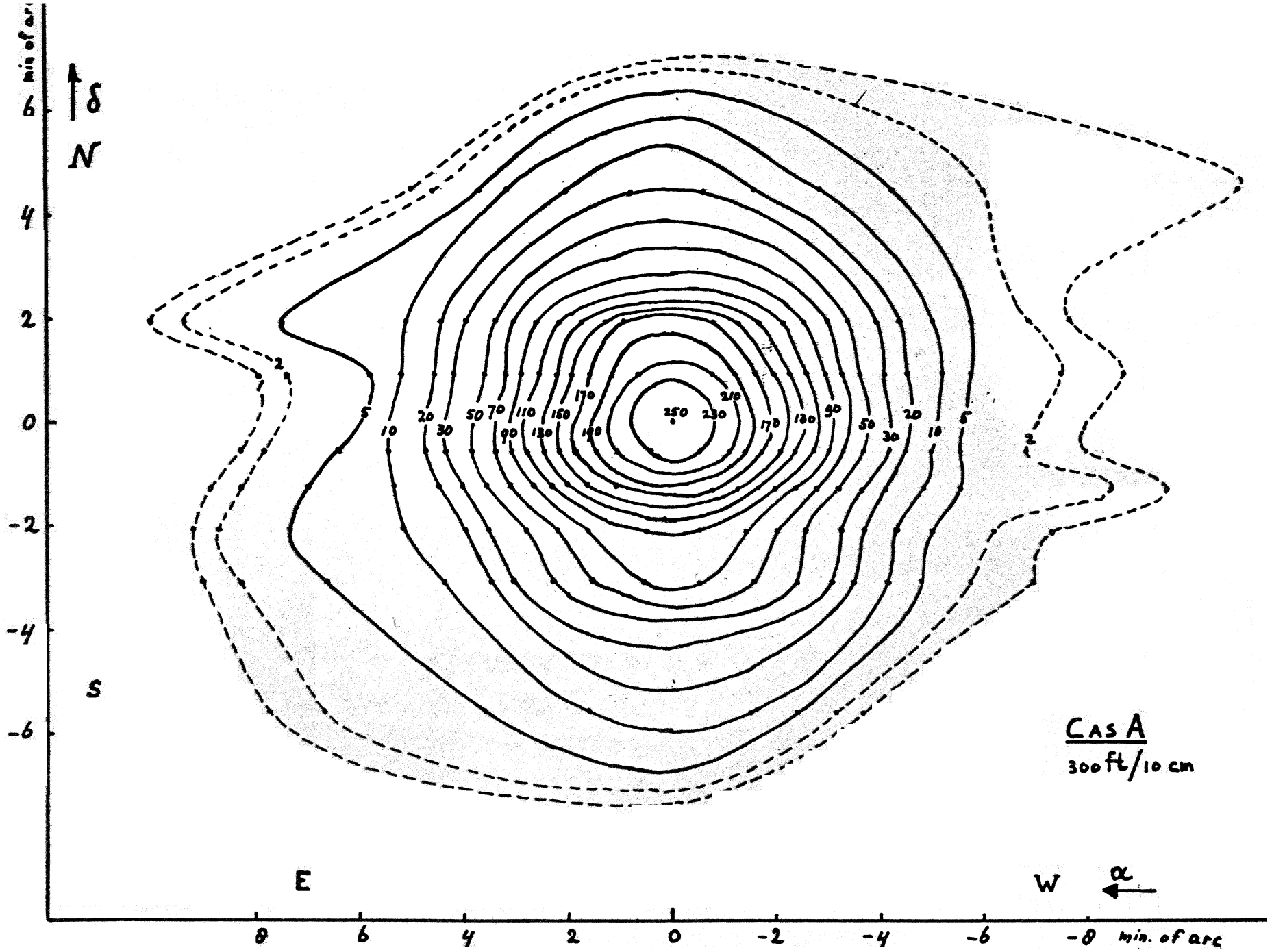

Fig. 5: Contour map representation of Cas A. One unit $\hat{=}$ 1 °K T_A.

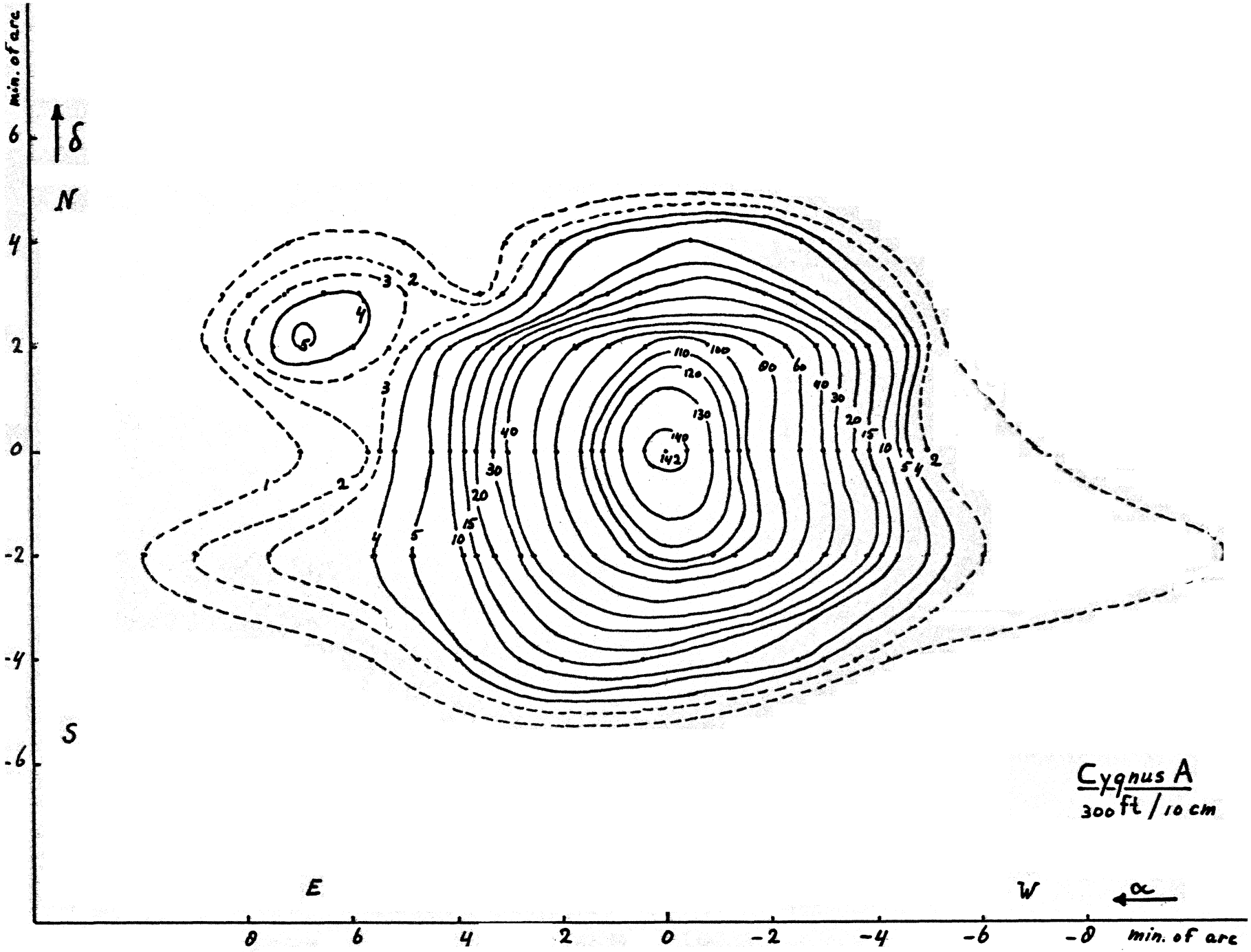

Fig. 8: Contour map of Cyg. A. One unit $\triangleq$ 1 °K T_A

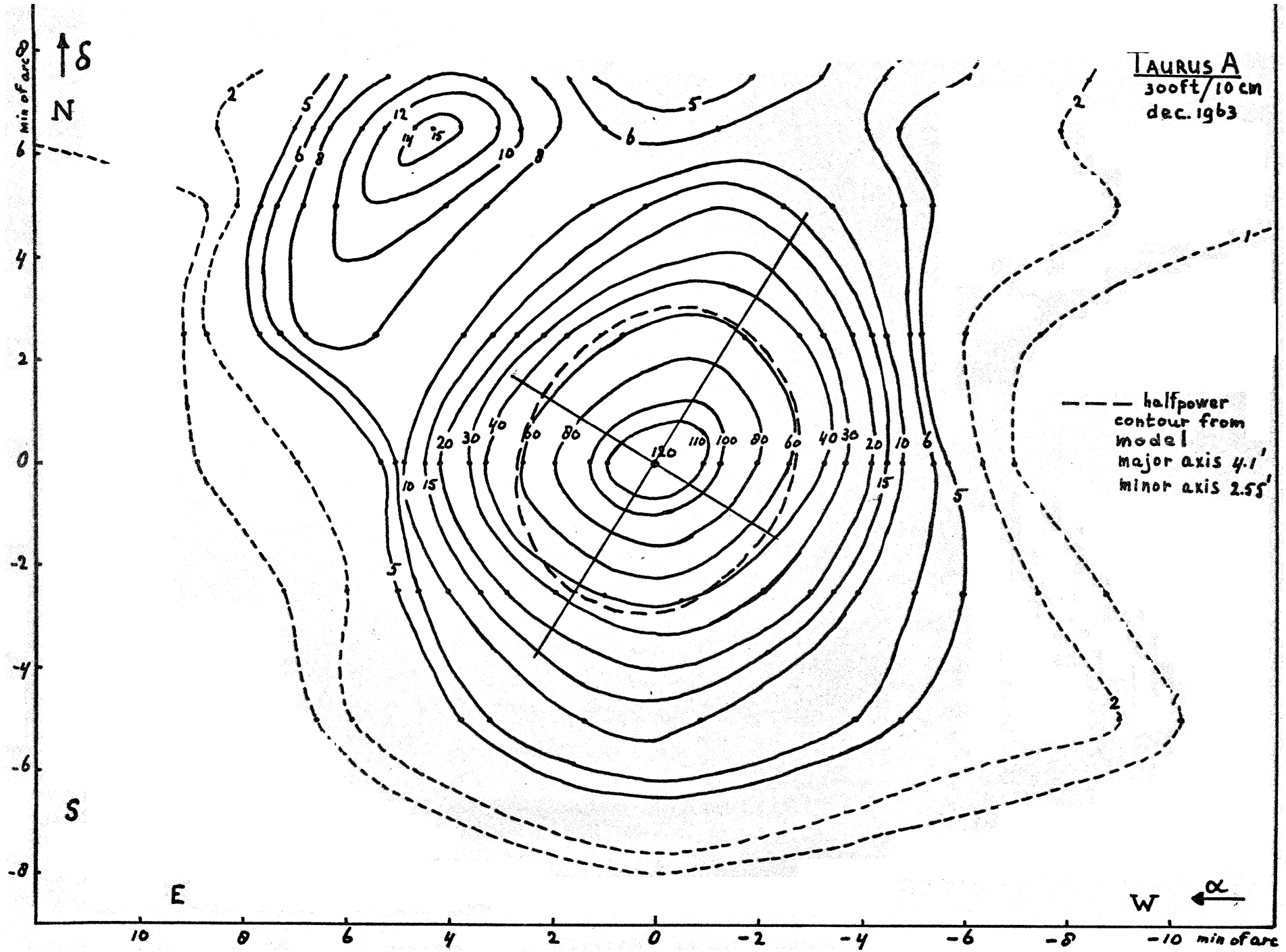

Fig. 11: Contour map of Tau A. One unit $\triangleq$ 1 °K T_A. The subsidiary maxima are caused by periodic distortions of the reflector surface.

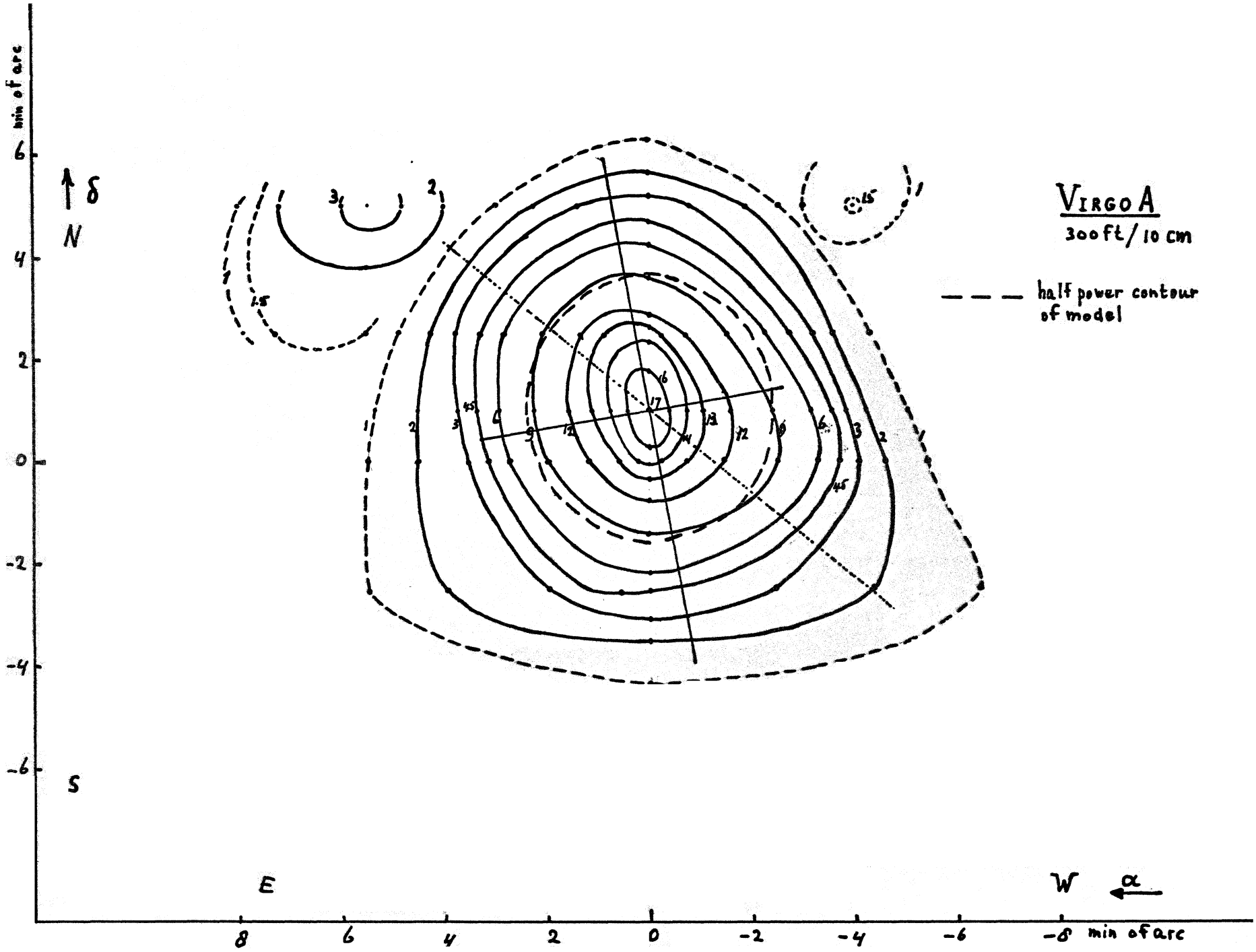

Fig. 14: Contour map of Virgo A. One unit $\triangleq$ 1 °K T_A. The subsidiary maxima are caused by periodic distortions of the reflector.

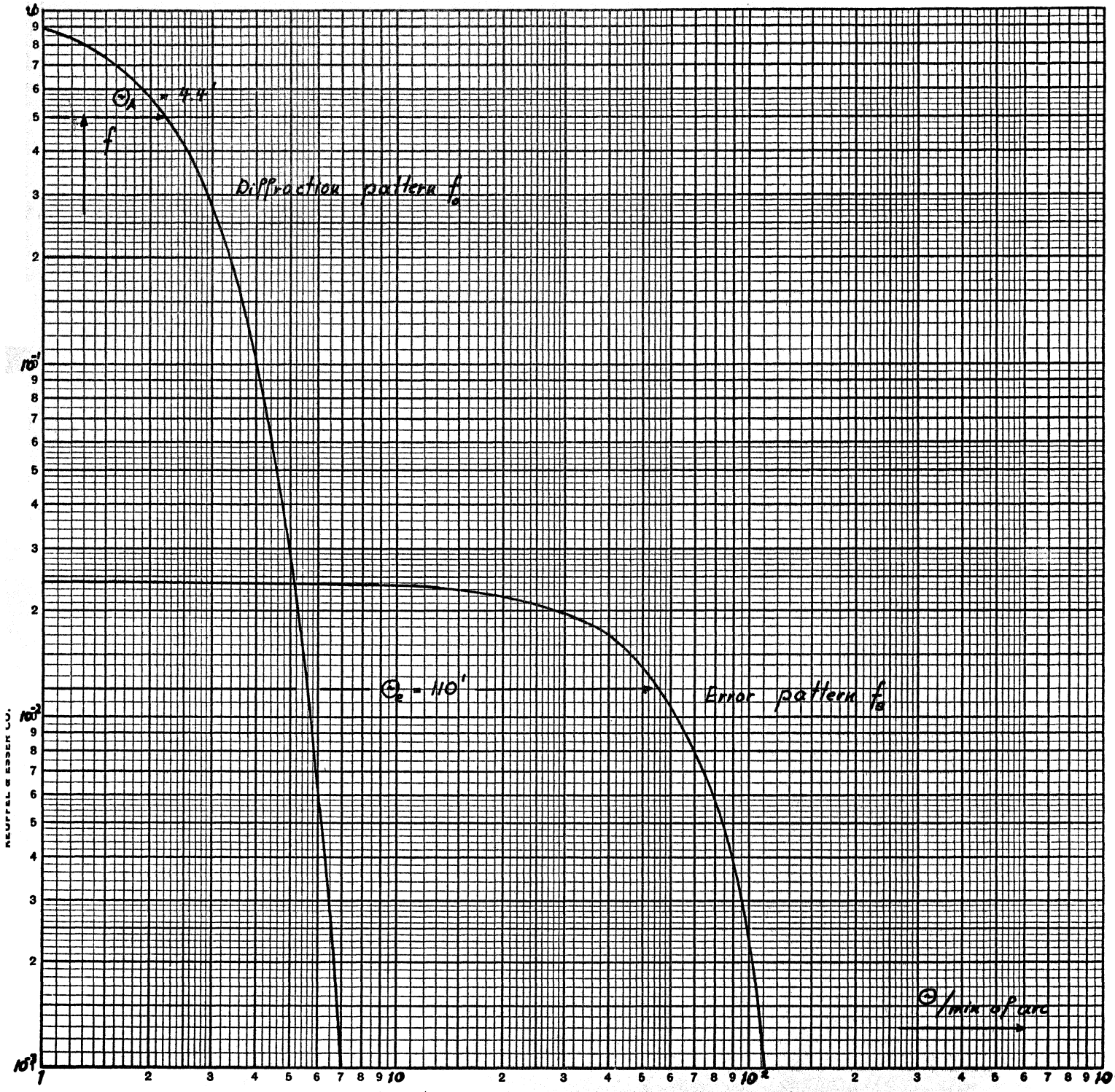

Fig. 23: Diffraction pattern and errors pattern of the 300-foot telescope at $\lambda = 10$ cm.

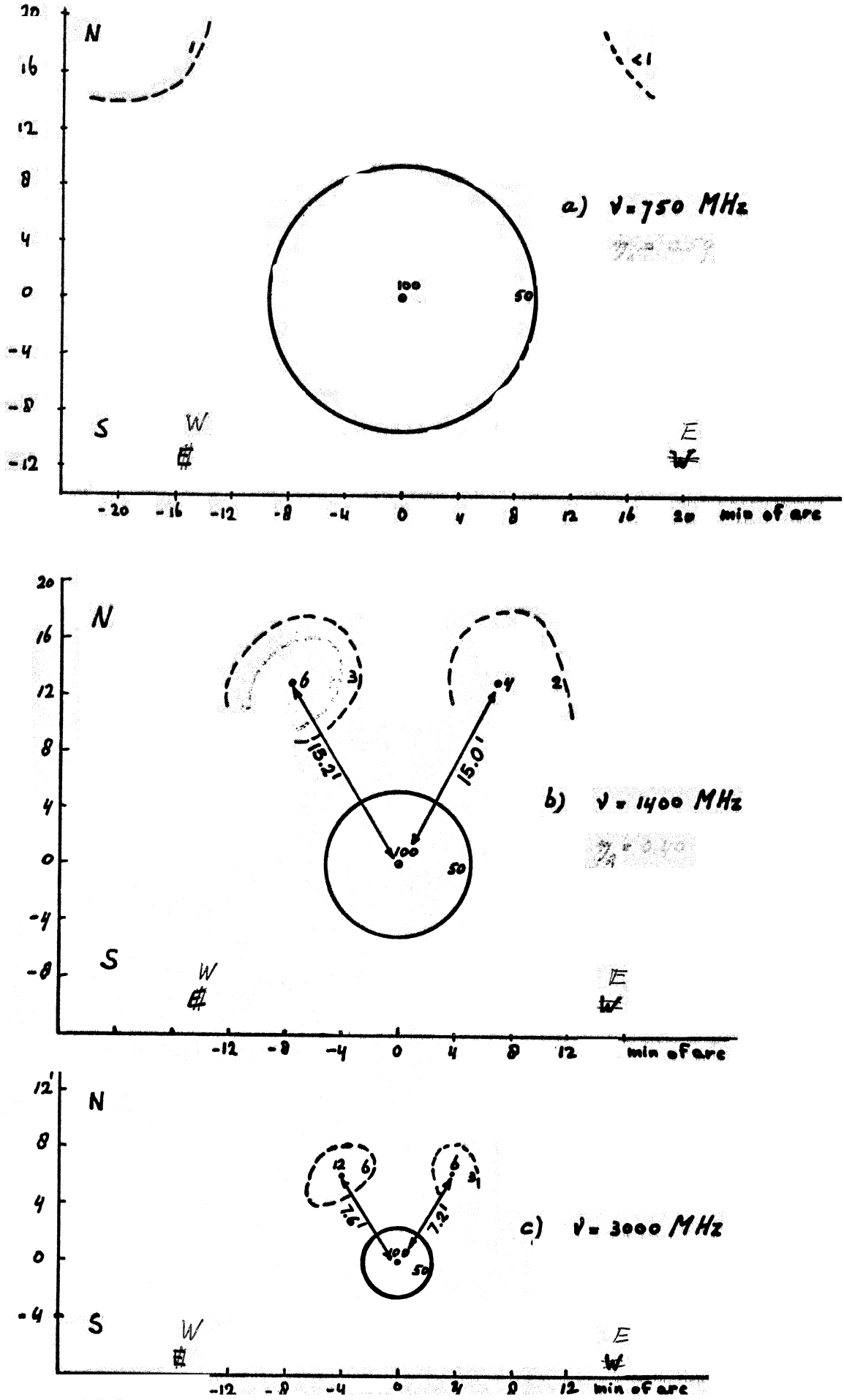

Figure 24: Center and half-power contours of the main lobe and two subsidiary maxima of the 300-foot telescope at 3 different frequencies.

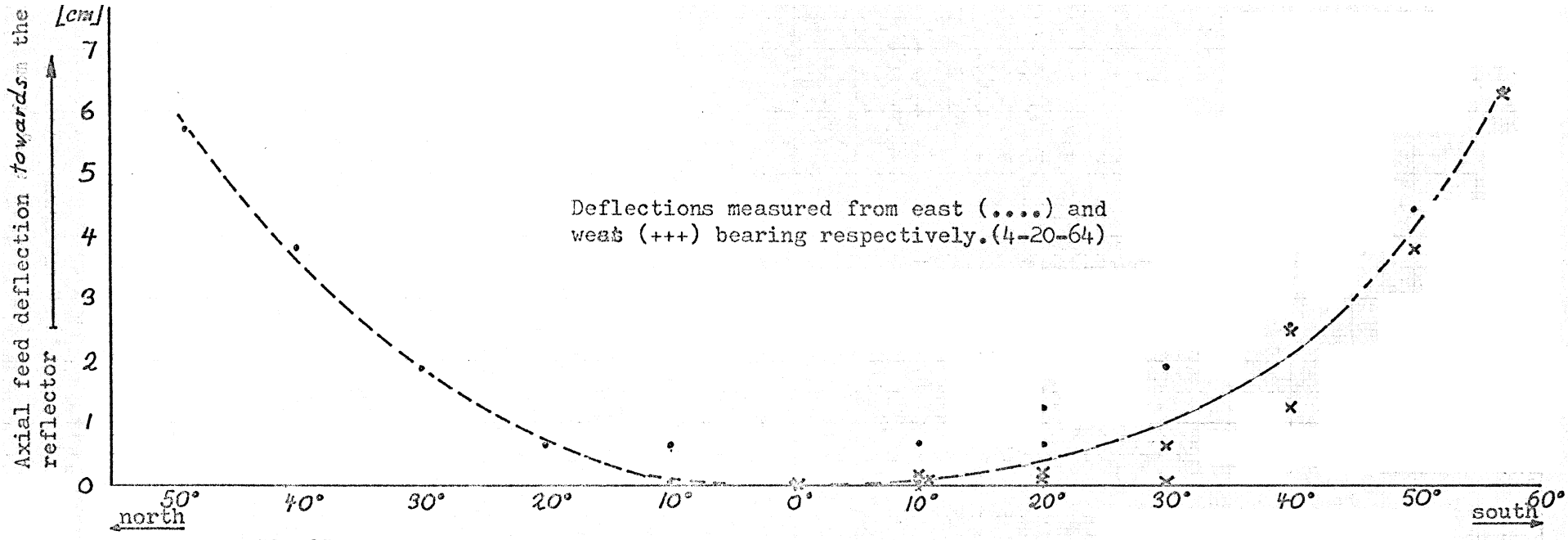

Fig.25b: Axial feed deflection as a function of zenith distance

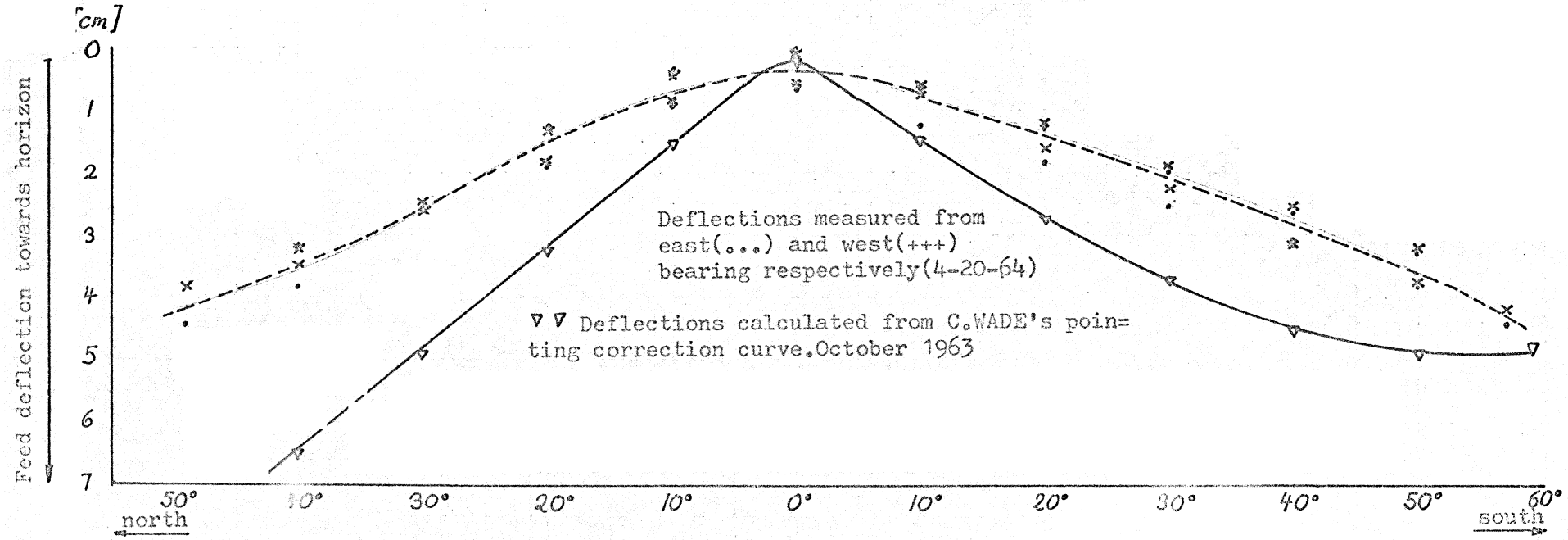

Fig.25a: Lateral deflection of the antenna feed in the 300-ft-reflector as a function of zenith distance

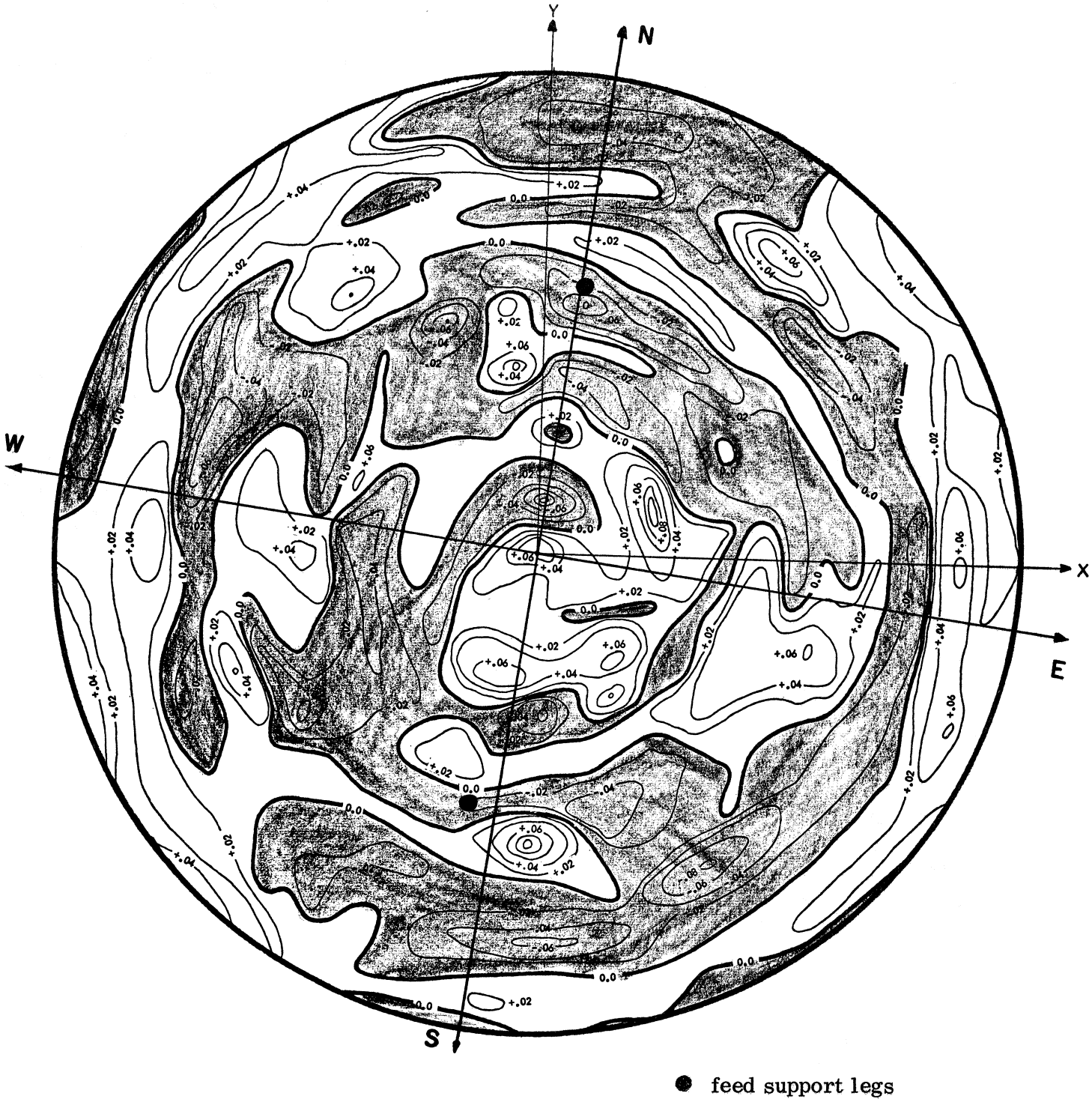

Fig. 26a: Contour map of the surface deviations of the 300-foot reflector at the zenith distance z = 0°. Shadowed areas correspond to (negative) deflections in the direction opposite to the focal point. (Contour intervals are 0.02 ft. = 6.1 mm.)

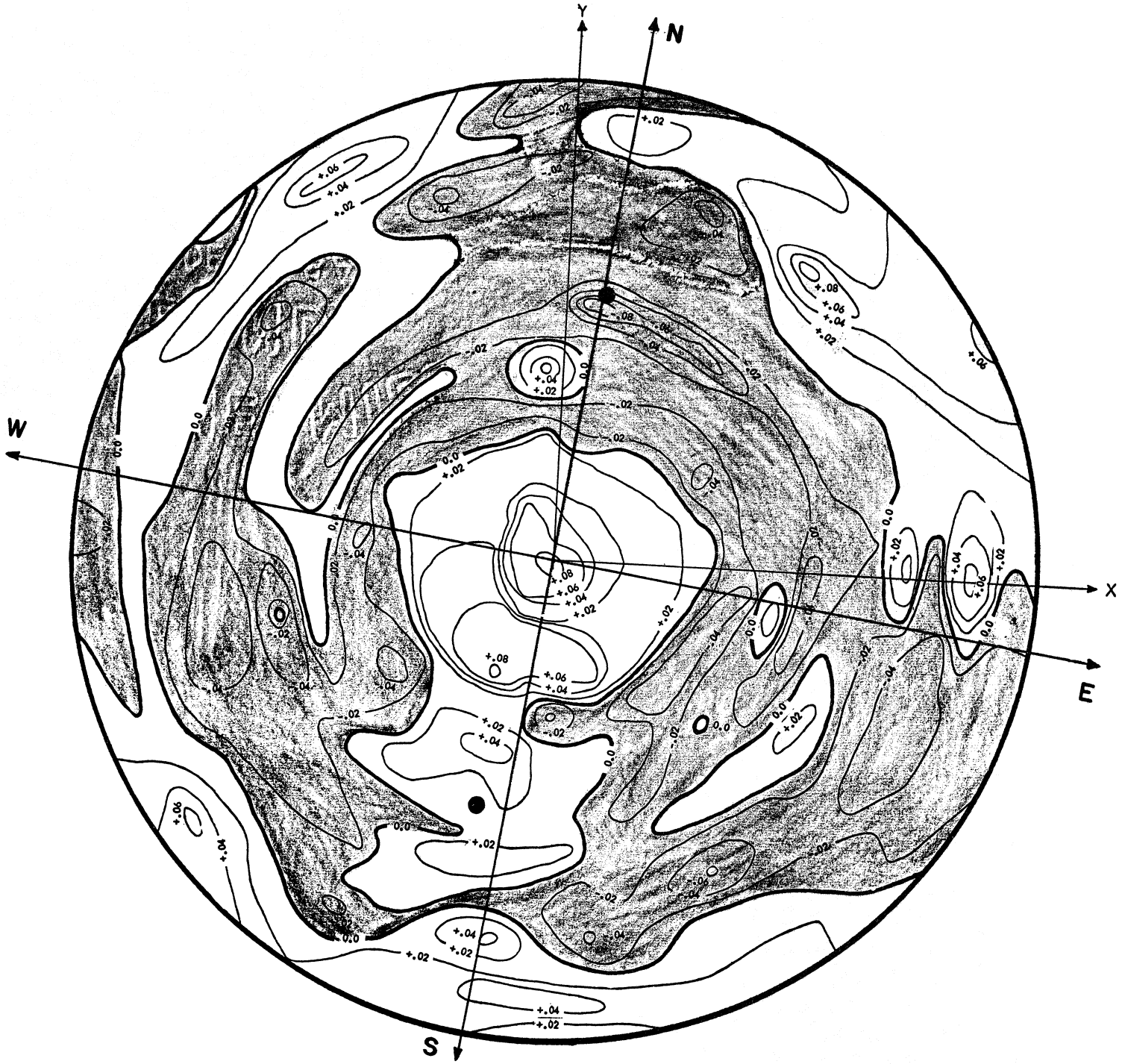

Fig. 26b: Contour map of the surface deviations of the 300-foot reflector at the zenith distance z = 30°. Shadowed areas correspond to (negative) deflections in the direction opposite to the focal point. The zero contour of this map has been corrected. (Contour intervals are 0.02 ft. = 6.1 mm.)

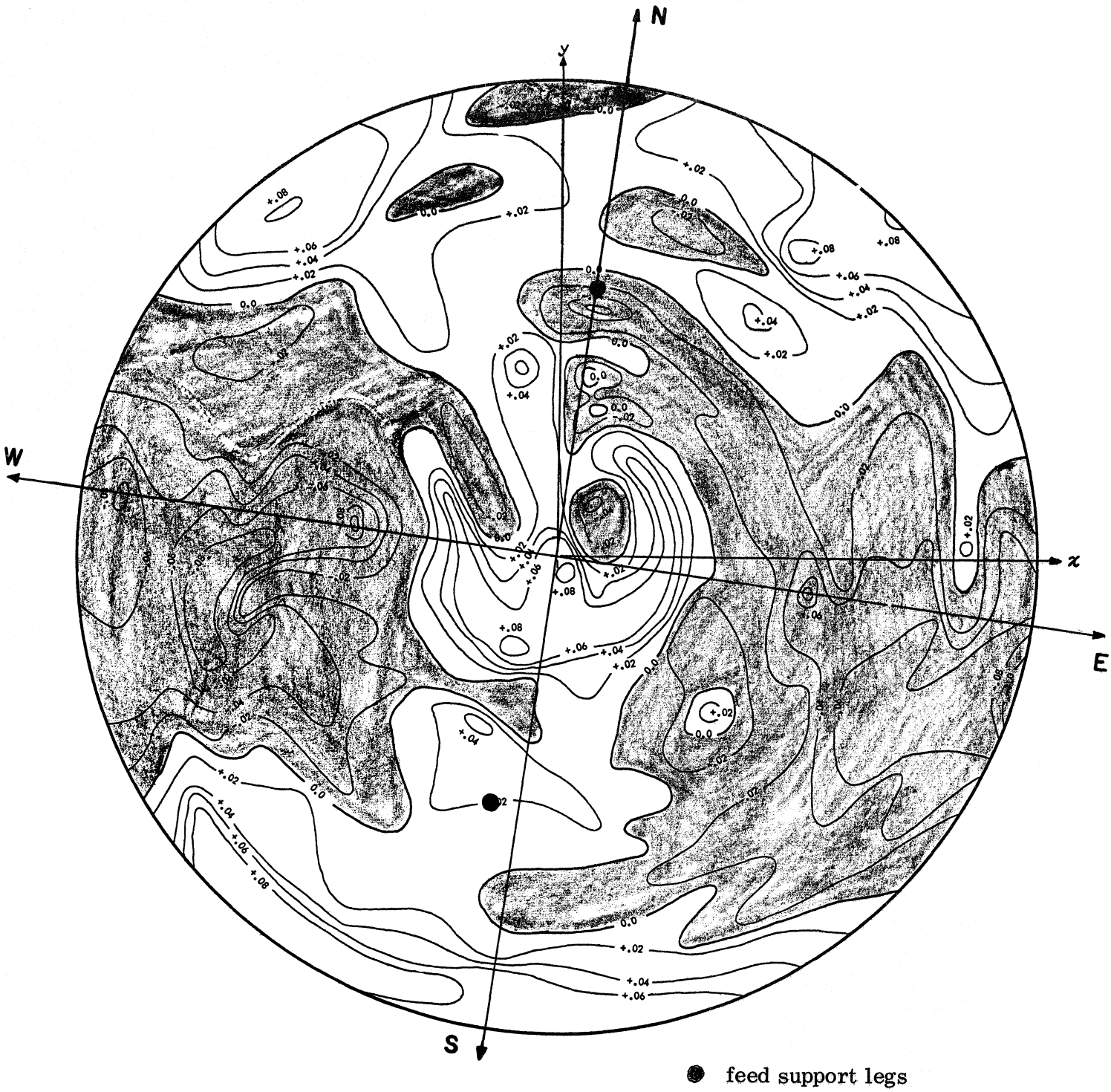

Fig. 26c: Contour map of the surface deviations of the 300-foot reflector at the zenith distance 51° 23' 40". Shadowed areas correspond to (negative) deflections in the direction opposite to the focal point. The zero contour of this map has been corrected. (Contour intervals are 0.02 ft. = 6.1 mm.)